

10-Iodo-11*H*-indolo[3,2-*c*]quinoline-6-carboxylic Acids Are Selective Inhibitors of DYRK1A

Hannes Falke,[†] Apirat Chaikuad,[‡] Anja Becker,[†] Nadège Loaëc,^{§,||} Olivier Lozach,^{||} Samira Abu Jhaisha,[⊥] Walter Becker,[⊥] Peter G. Jones,[#] Lutz Preu,[†] Knut Baumann,[†] Stefan Knapp,[‡] Laurent Meijer,^{*,§} and Conrad Kunick^{*,†}

[†]Institut für Medizinische und Pharmazeutische Chemie, Technische Universität Braunschweig, Beethovenstraße 55, 38106 Braunschweig, Germany

[‡]Nuffield Department of Clinical Medicine, Structural Genomics Consortium, University of Oxford, Old Road Campus Research Building, Roosevelt Drive, Headington, Oxford OX3 7DQ, U.K.

[§]ManRos Therapeutics, Perharidy Research Center, 29680 Roscoff, Bretagne, France

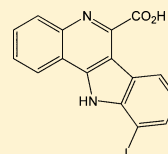
^{||}“Protein Phosphorylation and Human Disease” Group, Station Biologique de Roscoff, CNRS, 29680 Roscoff, France

[⊥]Institute of Pharmacology and Toxicology, RWTH Aachen University, Wendlingweg 2, 52074 Aachen, Germany

[#]Institut für Anorganische und Analytische Chemie, Technische Universität Braunschweig, Hagenring 30, 38106 Braunschweig, Germany

S Supporting Information

ABSTRACT: The protein kinase DYRK1A has been suggested to act as one of the intracellular regulators contributing to neurological alterations found in individuals with Down syndrome. For an assessment of the role of DYRK1A, selective synthetic inhibitors are valuable pharmacological tools. However, the DYRK1A inhibitors described in the literature so far either are not sufficiently selective or have not been tested against closely related kinases from the DYRK and the CLK protein kinase families. The aim of this study was the identification of DYRK1A inhibitors exhibiting selectivity versus the structurally and functionally closely related DYRK and CLK isoforms. Structure modification of the screening hit 11*H*-indolo[3,2-*c*]quinoline-6-carboxylic acid revealed structure–activity relationships for kinase inhibition and enabled the design of 10-iodo-substituted derivatives as very potent DYRK1A inhibitors with considerable selectivity against CLKs. X-ray structure determination of three 11*H*-indolo[3,2-*c*]quinoline-6-carboxylic acids cocrystallized with DYRK1A confirmed the predicted binding mode within the ATP binding site.



	5j (IC ₅₀)
DYRK1A:	6 nM
DYRK1B:	600 nM
DYRK2:	> 10000 nM
CLK1:	500 nM

■ INTRODUCTION

Down syndrome (DS) is one of the most frequent congenital disorders in humans. Individuals with DS exhibit a complex phenotype of structural alterations and intellectual disability. Many of them develop symptoms of Alzheimer's disease (AD) at a relatively young age, and a high proportion of DS individuals develop dementia at a later stage. DS is caused by a trisomy of chromosome 21 as a consequence of nondisjunction during meiotic cell division.^{1,2} Although the mechanisms leading from trisomy 21 to the clinical disease pattern are not yet understood, the 30 genes located in the so-called Down syndrome critical region (DSCR; 21q22.1–22.3) of chromosome 21 are highly likely to be associated with the disease.^{3–5} There is mounting evidence that overexpression of DYRK1A (dual-specificity tyrosine phosphorylation-regulated kinase 1A), a protein kinase encoded by a gene located within DSCR, contributes to mental retardation in DS. Since DYRK1A is also connected to neurological disorders such as AD,^{6,7} the early onset of AD in DS individuals has been related to DYRK1A overexpression.⁸ Two histopathological features are found in the brains of AD patients: extracellular β -amyloid plaques and

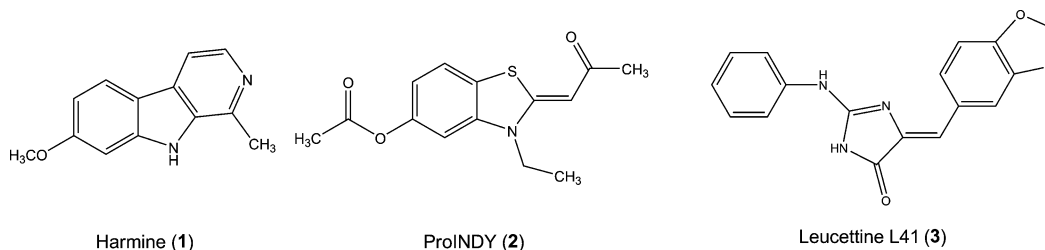
intracellular tangles consisting of hyperphosphorylated tau protein.⁹ DYRK1A appears to connect these biochemical aberrations.¹⁰ Hyperphosphorylation of tau by DYRK1A diminishes its microtubule-stabilizing effects and increases aggregation.¹¹ The neurological impairment of mice with modified DYRK1A expression has also been attributed to deregulated splicing, leading to an imbalance of 3R-tau and 4R-tau isoforms.^{12,13} The increased 3R-tau concentration (by a factor of up to 4) observed in DS has been associated with changes of the neuronal cytoskeleton and neurofibrillary degeneration.¹² DYRK1A-overexpressing mice also exhibit increased production of A β peptide, which has been attributed to phosphorylation of the amyloid precursor protein (APP) and presenilin 1 by DYRK1A.^{14,15}

DYRK1A is a member of the DYRK protein kinases (DYRK1A, DYRK1B, DYRK2, DYRK3, DYRK4), which are part of the CMGC superfamily and share structural similarity of the catalytic domain and a small sequence nearby, the so-called

Received: December 23, 2014

Published: March 2, 2015

Chart 1. Three Reported DYRK1A Inhibitors



DYRK homology box (DH-box).¹⁶ Although DYRKs are serine/threonine kinases, autophosphorylation occurs at a conserved tyrosine residue of the activation loop. This autophosphorylation is constitutive and seems to be not related to regulation.^{17,18} In the light of its involvement in DS and other neurodegenerative disorders, the inhibition of DYRK1A with small chemical inhibitors has been suggested as a therapeutic strategy.^{19,20} Selective DYRK1A inhibitors would also be valuable tools for the investigation of the role of DYRK1A in physiological and pathobiochemical processes. To date, most protein kinase inhibitors exert their activity by competing with ATP in the binding pocket of the kinase. Since ATP binding sites of protein kinases share a common structure with subtle differences, selectivity with regard to closely related kinases is not easily achieved.^{21,22} When selective DYRK1A inhibitors are to be developed, special attention should therefore be devoted to other members of the CMGC superfamily, consisting of CDKs, MAPkinases (such as ERKs), GSK-3, and CDC-like kinases.²³

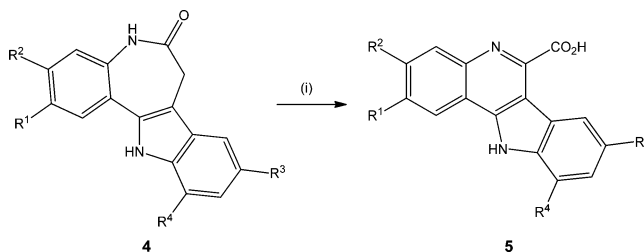
The structures and properties of DYRK1A inhibitors have been summarized in recent reviews.^{19,24} A well established DYRK1A inhibitor is the β -carboline alkaloid harmine (**1**, Chart 1), which however also shows high affinity for serotonin and tryptamine receptor binding sites,²⁵ acts as monoamine oxidase A (MAO A) inhibitor,²⁶ and also inhibits CLKs²⁷ and therefore is inappropriate for use as a cellular chemical probe. Epigallocatechin 3-gallate (EGCG) is a polyphenolic constituent of green tea reported to inhibit DYRK1A in a non-ATP-competitive manner,^{28,29} but it is chemically reactive and also interacts with numerous intracellular signaling pathways by other mechanisms.³⁰ The benzothiazole derivative INDY showed potent inhibition of DYRK1A and related kinases (DYRK1B, DYRK2, DYRK3, CLK1, CLK4, CK1, and PIM1). A prodrug of this compound, proINDY (**2**), has been shown to protect *Xenopus* tadpoles that overexpress DYRK1A against head malformation during development.²⁷ Leucettine L41 (**3**), derived from the marine natural product leucettamine B, is an ATP-competitive inhibitor of DYRKs and CLKs that also interacts with GSK-3 and CK2 to a lower extent. It modulates pre-mRNA splicing, protects HT22 hippocampal cells from glutamate-induced cell death, induces autophagy, and inhibits phosphorylation of tau on Thr212.^{31–33} Similar to the agents mentioned before, the recently reported chemical DYRK1A inhibitors comprising meridianines,³⁴ indirubin 5'-carboxylates,³⁵ thiazolo[5,4-*f*]quinazolines,³⁶ pyrido[2,3-*d*]pyrimidines,³⁷ 3,5-diaryl-7-azaindoles (DANDYs),³⁸ KH-CB19,³⁹ 2,4-bisubstituted thiophenes,⁴⁰ and hydroxybenzothiophenes⁴¹ either show limited selectivity against structurally closely related DYRK and CLK kinase isoforms or were not tested on these enzymes. In this regard, a DYRK1A inhibitor with high selectivity over other CMGC kinases would be useful for biochemical and cellular studies and as lead motif for the

development of new pharmaceuticals targeting neurodegenerative diseases. To identify novel hit matter, we tested a small diverse in-house compound library against DYRK1A and the following CMGC protein kinases: CDK1/cyclin B, CDK2/cyclin A, CDK5/p25, CK1, GSK-3, and ERK2. The only compound showing a moderate selective DYRK1A inhibition ($IC_{50} = 2.6 \mu M$) was the 11*H*-indolo[3,2-*c*]quinoline-6-carboxylic acid **5a** (Table 1).

SYNTHESIS AND EVALUATION OF ANALOGUES

In order to generate congeners of **5a** with increased potency, we synthesized a number of analogues **5b–h**, starting from the readily available 7,12-dihydroindolo[3,2-*d*][1]benzazepin-6(5*H*)-ones **4** (paullones), a class of dual GSK-3/CDK inhibitors^{42–53} that undergo a radical-induced rearrangement when stirred with Co(II) acetate and *N*-hydroxyphthalimide (NHPI) in the presence of oxygen⁵⁴ (Scheme 1).

Scheme 1. Synthesis of 11*H*-Indolo[3,2-*c*]quinoline-6-carboxylic Acids **5** by Rearrangement of Paullones **4**^a



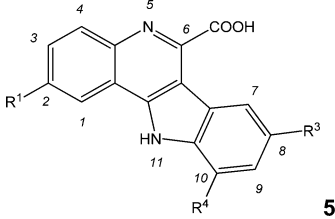
^aReagents and conditions:⁵⁴ Co(II) acetate, NHPI, air or O₂, DMF, room temperature to 70 °C (13–88%).

Evaluation of these derivatives in the kinase panel revealed that substituents located in 8-position of the heterocyclic scaffold eliminated the DYRK1A inhibitory activity, suggesting steric exclusion from the ATP-binding pocket, the most likely binding site of the inhibitors. Compounds with polar H-bond acceptor substituents in 8-position were moderate and selective GSK-3 inhibitors but also were inactive on DYRK1A. Strikingly, the 10-chloro derivative **5h** showed that DYRK1A inhibitory potency increased by 2 orders of magnitude ($IC_{50} = 31 \text{ nM}$) compared to **5a** without inhibiting other kinases of the panel displayed in Table 1.

In light of the results shown in Table 1, we hypothesized that substituents in 10-position of the parent scaffold induce a strong and selective inhibitory activity of DYRK1A.

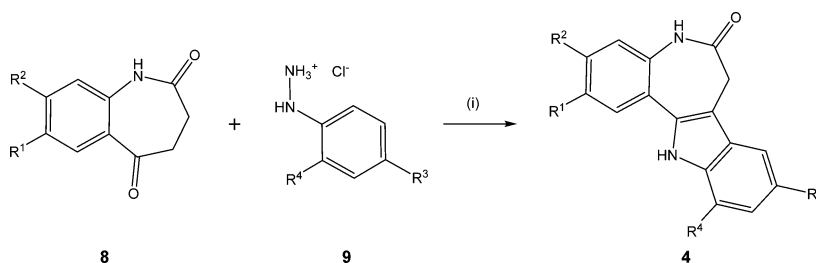
CHEMISTRY

To expand the panel of potential selective DYRK1A inhibitors and to gain insight into SAR, a series of 10-substituted 11*H*-indolo[3,2-*c*]quinoline-6-carboxylic acids **5h–w** and the hetero-

Table 1. Kinase Inhibitory Activity (IC_{50} , μM) of 11*H*-Indolo[3,2-*c*]quinoline-6-carboxylic Acids **5a–h** on a Panel of Selected CMGC Protein Kinases^a


compd	R ¹	R ³	R ⁴	IC_{50} , μM						
				CDK1	CDK2	CDK5	CK1	DYRK1A	GSK-3	ERK2
5a	H	H	H	>10	>10	>10	>10	2.6	>10	>10
5b	H	C(CH ₃) ₃	H	>10	>10	>10	>10	>10	>10	>10
5c	H	CF ₃	H	>10	>10	>10	>10	>10	>10	>10
5d	H	NO ₂	H	>10	>10	>10	>10	>10	0.82	>10
5e	H	CH ₃	H	>10	>10	>10	>10	>10	>10	>10
5f	H	COOH	H	>10	>10	>10	>10	>10	0.35	>10
5g	I	Cl	H	>10	>10	>10	>10	>10	>10	>10
5h	H	H	Cl	>10	>10	>10	>10	0.031	>10	>10

^aAll data points for construction of dose–response curves were recorded in triplicate. Typically, the standard deviation of single data points was below 10%. For test conditions refer to the section Experimental Procedures.

Scheme 2. Synthesis of Paullones **4**^a

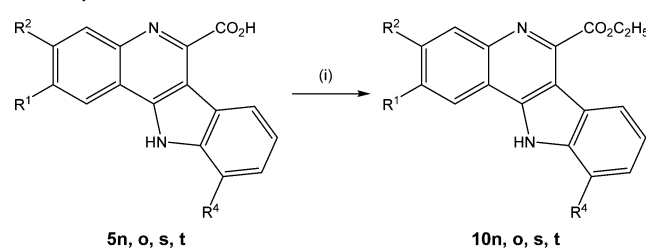
^aReagents and conditions: (i) (1) AcOH, NaOAc, 70 °C, (2) AcOH, H₂SO₄, 70 °C. For residues R¹–R⁴ refer to Tables 1 and 2.

cyclic congeners **6** and **7** were synthesized from paullones **4** (or appropriate heterocyclic paullone analogues), applying a method analogous to Scheme 1. All paullones **4** used in this paper as starting materials were prepared from suitable 3,4-dihydro-1*H*-1-benzazepine-2,5-diones **8** and phenylhydrazines **9** by standard Fischer indole synthesis procedures described earlier (e.g., Scheme 2).^{43–45,51,54–56}

The esters **10n,o,s,t** were synthesized by treatment of the appropriate carboxylic acids **5n,o,s,t** with ethanolic hydrogen chloride at room temperature (Scheme 3). An X-ray structure analysis of the ester **10o** unambiguously confirmed the structure which was present as its monohydrate in the isolated crystals (Figure 1).

■ BIOLOGICAL EVALUATION AND DISCUSSION

The new derivatives **5h–w** and heterocyclic analogues **6** and **7** were tested on an extended panel of CMGC kinases comprising several DYRK and CLK isoforms (Table 2). Evaluation of the results yielded a consistent activity/selectivity pattern depending on the substituent in position 10. All compounds with a 10-chloro substitution (**5h,m,p,q,s,u–w**, **6**) exhibited DYRK1A inhibitory activity with IC_{50} values in double digit nanomolar to single digit micromolar concentrations. However, similar to other DYRK1A inhibitors, the selectivity of these compounds was low and other DYRKs (DYRK1B, DYRK2), CLKs (CLK1, -2, -4), and CDK9 were also inhibited at comparable

Scheme 3. Synthesis of Ethyl 11*H*-Indolo[3,2-*c*]quinoline-6-carboxylates **10**^a

^aFor substitution pattern, refer to Table 2. Reagents and conditions: (i) EtOH, HCl (g), room temperature, 30 min (27–75%).

concentrations. The lack of DYRK1A/CLK1 selectivity also applied to the heterocyclic analogues **6** and **7**. All tested derivatives showed selectivity versus CDKs 1, 2, 5 and CLK3. Within series **5**, substitution of the 10-chloro substituent by fluorine led to weaker activity (cf. **5l**) or complete loss (cf. **5r**) of kinase inhibitory activity. Derivatives in which the 10-chloro substituents were replaced by bromine (e.g., **5i**, **5n**, **5t**) showed a slightly improved DYRK1A inhibition but with diminished selectivity versus DYRK2. It is noteworthy that the 10-bromo substituted 1-aza analogue **7** did not inhibit DYRK2 but did inhibit CLKs 1, 2, and 4, which are frequently affected by DYRK1A inhibitors. The introduction of a 10-iodo substituent

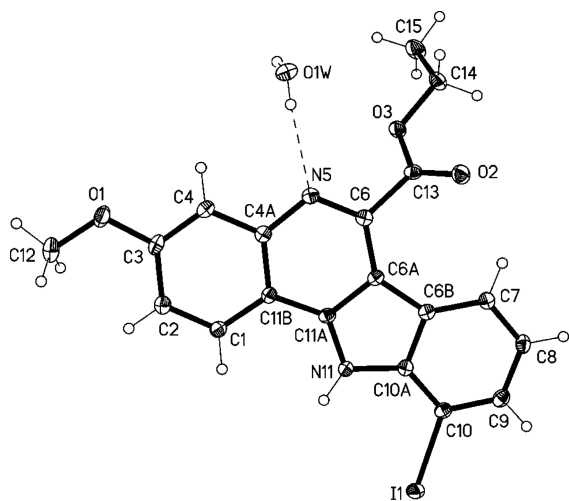


Figure 1. Crystal structure of the ethyl ester **10o** as its monohydrate.

(compounds **5j** and **5o**) eventually led to the desired properties. These compounds showed strong potency (DYRK1A IC_{50} of 6 and 22 nM, respectively) and good selectivity, as all tested competing kinases were inhibited by **5j** and **5o** in concentrations higher by at least 2 orders of magnitude. The selectivity for DYRK1A over DYRK1B is particularly striking, since the catalytic domains of these kinases are very closely related on the level of the amino acid sequence (85% sequence identity). Upon replacement of the 10-halogen by a methoxy group the DYRK1A inhibitor **5k** was produced, which also inhibited CDK9, and therefore 10-methoxy-substituted derivatives were not further pursued. The finding that the carboxylic acid esters **10n,o,s,t** failed to inhibit any of the tested kinases underlines the importance of the free carboxylic acid moiety at the 6-position of the molecule.

To evaluate the most potent and rather selective DYRK1A inhibitor **5j** in a cellular assay, we analyzed its effect on the phosphorylation of Thr434 in splicing factor 3B1 (SF3B1) in HeLa cells. Phosphorylation of this site depends on DYRK1A and serves as a useful indicator of the activity of the cellular endogenous DYRK1A.^{57,58} In this assay **5j** dose-dependently reduced the phosphorylation of Thr434 in SF3B1, showing its DYRK1A-inhibitory effect in living cells (Figure 2A). Next we analyzed the effect of **5j** on tau protein as a potentially relevant target in AD. Overexpression of DYRK1A in HEK293 cells caused an increased phosphorylation of tau at Thr212, which was inhibited by **5j** with an IC_{50} of 2.1 μ M (Figure 2B). The high concentration margin between in vitro and cellular DYRK1A inhibition by **5j** is probably the result of poor cellular uptake. Nevertheless, the potency of **5j** as an inhibitor of tau phosphorylation is in the same range as or better than those of other DYRK1A inhibitors that were tested in this assay.^{27,59}

The relationship between molecular structure and DYRK1A inhibition indicated a high significance of the halogen substitution in position 10 of the title compounds. The fact that on the one hand in the series **5h–j** the iodo substituted derivative **5j** exhibited the highest potency and on the other hand iodine shows the highest tendency to form halogen bonds with carbonyl oxygen atoms hints to halogen bond involvement in this area. However, the data collected with the derivatives described in this report are not sufficient to substantiate such a hypothesis. For example, in the 3-methoxy substituted series

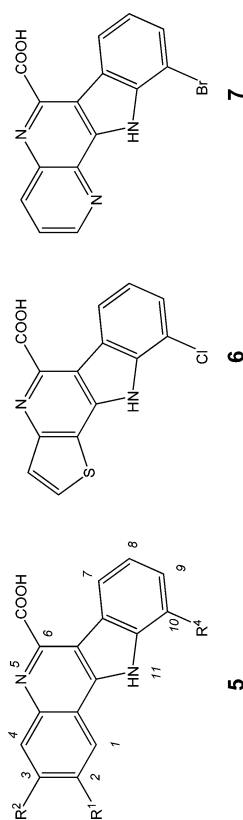
5m–o the DYRK1A inhibition is independent of halogen nature. Further evidence against the necessity of a halogen bond in this position is the 10-methoxy derivative **5k**, which despite lacking a halogen retains DYRK1A inhibitory activity. For a better understanding of the ligand–target interaction mode, docking studies and X-ray structure analyses were performed with representative congeners.

DOCKING STUDIES

Because the majority of protein kinase inhibitors act by competition with ATP at its binding site, we assumed this binding mode also for inhibitors of series 5. For the construction of a detailed model of the inhibitor–protein interaction, representatives of series 5 were docked into a published DYRK1A structure (PDB code 2WO6), the ATP pocket of which is occupied by the ligand DJM2005.⁶⁰ As a control, redocking DJM2005 into chain B of the protein reproduced the original pose of the inhibitor, albeit not as the highest ranked pose. Docking of **5i** into the ATP binding pocket produced four different poses as the highest ranked results (Figure 3). Although lacking the classical acceptor–donor–acceptor hydrogen bond pattern between the hinge region of the kinase and the inhibitor, the pose in Figure 3b was assessed as the most plausible, since it not only comprises a salt bridge between the carboxylate and the protonated ϵ -amino group of the conserved lysine but, compared to the orientation in Figure 3a, accommodates a larger part of the molecule in the binding pocket. Another convincing argument in favor of orientation in Figure 3b was its high similarity to the orientation of the inhibitor IRB in DYRK2 (PDB code 3KVW, not depicted here). Although the program used for docking (GOLD, versions 4.0 and 5.1, respectively) was not taking halogen bonding into account, the contact between the bromo substituent in 10-position and the carbonyl oxygen of Leu241 as shown in Figure 3b resembled an atom alignment found with halogen bonds. It had been reported before that halogen bonds may replace the canonical hinge–inhibitor hydrogen-bond interaction.^{39,61–64} However, given the uncertainty encountered with docking experiments, in this case the resulting pose was not adequate to prove the de facto existence of a halogen bond.

CRYSTAL STRUCTURE ANALYSIS

In order to validate our docking hypothesis experimentally, we cocrystallized DYRK1A with the compounds **5s**, **5t**, and **5j** as examples of chloro, bromo, and iodo substituted congeners (Table 3, Figure 4). In all cases the orientation in Figure 3B generated by the docking experiment was confirmed. Figure 4A–C illustrates the binding modes of these three inhibitors in the ATP binding site. In **5s** and **5t**-DYRK1A complexes, the iodide groups at the position 2 (R^1) were observed to partially or completely fall off from the main inhibitor scaffold with the free radicals still located adjacent to its original position. Overall, the crystal structure revealed that the inhibitor was kept in position by a salt bridge between the carboxylate and the conserved lysine 188. As expected, the binding mode was highly conserved in all three inhibitor complexes. A water-mediated network of hydrogen bonds involving Ser242 and Asp307 probably contributed to the binding affinity of the ligands. The P-loop residue Phe170 flipped into the ATP binding site potentially forming aromatic end-on stacking interactions with the inhibitor.

Table 2. Inhibition of CMGC Protein Kinases (IC_{50} , μM) by 11H-Indolo[3,2-c]quinoline-6-carboxylic Acids 5h–w and by Heterocyclic Analogues 6 and 7^a

compd	IC_{50} , μM																
	R ¹	R ²	R ⁴	CDK1	CDK2	CDK5	CDK9	CKI	GSK-3	CLK1	CLK2	CLK3	CLK4	DYRK1A	DYRK1B	DYRK2	DYRK3
5h	H	H	Cl	>10	>10	>100	0.150	>100	>100	0.130	0.061	>100	0.045	0.031	0.210	0.040	>100
5i	H	H	Br	>100	>100	>100	0.160	>100	>100	0.032	0.055	>100	0.035	0.020	0.080	0.016	>100
5j	H	H	I	>10	>10	>10	>10	>10	>10	0.50	5.5	>10	0.21	0.006	0.600	>10	>10
5k	H	H	OMe	>10	>10	>10	0.120	>10	>10	1.1				0.032			
5l	H	OMe	F	>10	>10	>10	>10	>10	>10	0.33	0.18	>10	0.21	0.32	3.0	8.00	2.3
5m	H	OMe	Cl	>10	>10	>10	1.000	>10	>100	0.025	0.390	>10	0.068	0.023	1.000	0.0330	>10
5n	H	OMe	Br	>10	>10	>10	1.500	>10	3.300	0.0210	0.1100	>10	0.042	0.018	0.230	0.023	1.4
5o	H	OMe	I	>10	>10	>10	>10	>10	>10	2.0	>10	>10	2.3	0.022	>10	>10	>10
5p	H	Cl	Cl	>10	>10	>10	>10	>10	>10	0.94				2.3			
5q	H	OEt	Cl	>10	>10	>10	>10	>10	2.2	0.24	>10	>10	0.35	2.0	>10	>10	>10
5r	I	H	F	>10	>10	>10	>10	>10	>10	>10	>10	>10	>10	>10	>10	>10	>10
5s	I	H	Cl	>10	>10	>10	2.2	>10	>10	3.4	1.3	>10	3.6	0.18	4.9	0.22	>10
5t	I	H	Br	>10	>10	>10	1.5	>10	8.8	1.2	0.61	>10	1.1	0.12	1.4	0.13	>10
5u	OCH ₃	H	Cl	>10	>10	>10	0.21	2.3	3.0	0.10				0.039			
5v	3-MeOPh	H	Cl	>10	>10	>10	3.1	>10	>10	0.22	0.51	>10	>10	0.041	1.9	0.079	0.3
5w	4-MeOPh	H	Cl	>10	>10	>10	>10	>10	>10	0.30				0.056			
6	na	na	na	>10	>10	>10	0.350	>10	4.300	0.053				0.17			
7	na	na	na	>10	>10	>10	2.0	>10	>10	0.28	1.1	>10	0.37	0.13	1.300	>10	>10

^aAll data points for construction of dose–response curves were recorded in triplicate. Typically, the standard deviation of single data points was below 10%. A space indicates that the compound was not tested on the indicated kinase. For test conditions refer to the section Experimental Procedures. na = not applicable.

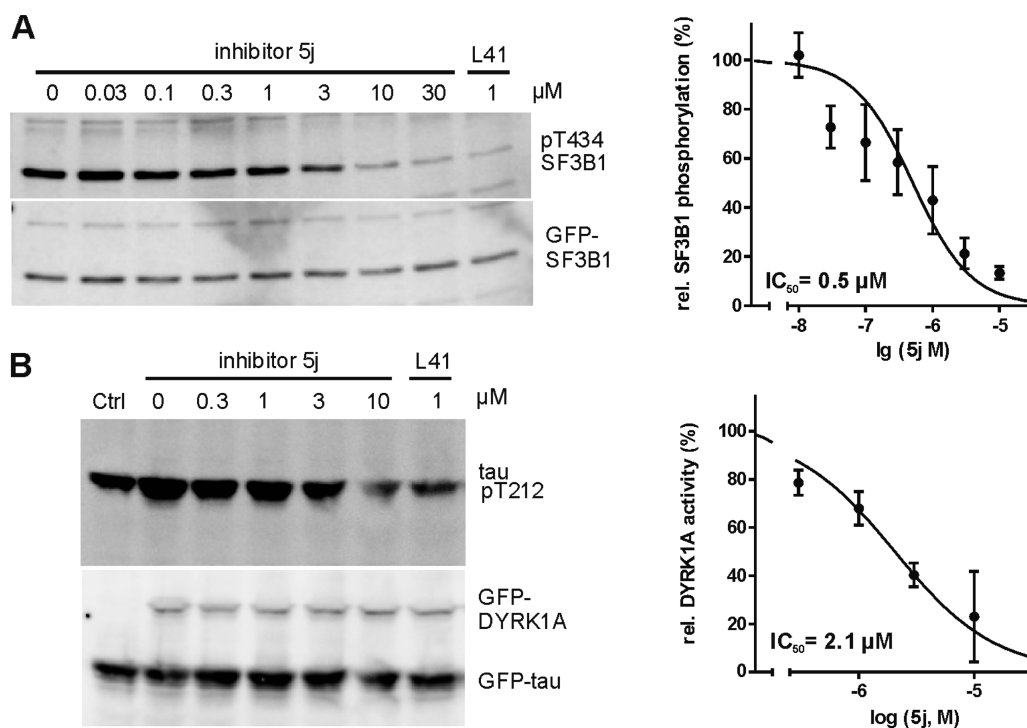


Figure 2. Efficacy of compound **5j** in cell-based assays. (A) HeLa cells expressing GFP-SF3B1 were treated with compound **5j** or the reference inhibitor leucettine 41 (L41) as indicated. Phosphorylation of SF3B1 was determined by immunoblotting with a pThr434 antibody, and expression levels of GFP-SF3B1 were assessed with GFP antibody. The left panel shows Western blots of a representative experiment, and the graph presents the quantitative evaluation of three experiments as the mean values of normalized pThr434 immunoreactivity relative to that in untreated cells \pm SEM. (B) Stably transfected HEK293-tau-DYRK1A cells⁵⁹ were treated with doxycyclin (except lane 1, Ctrl) to induce the expression of GFP-DYRK1A and compound **5j** or the reference inhibitor leucettine 41 (L41). Phosphorylation of tau on Thr212 (pT212) was detected by immunoblotting with a phosphospecific antibody, and expression levels of the recombinant proteins were determined with a GFP antibody. To correct for basal tau phosphorylation not caused by DYRK1A, the pT212 immunoreactivity in L41 treated cells was subtracted as background. The graph presents the results of three experiments as the mean values of pThr212 immunoreactivity relative to that in untreated cells \pm SEM. Curve fitting yielded $IC_{50} = 0.5 \mu\text{M}$ (95% confidence interval 0.3–0.8 μM) for the inhibition of SF3B1 phosphorylation and $IC_{50} = 2.1 \mu\text{M}$ (95% confidence interval 1.2–3.6 μM) for the inhibition of tau phosphorylation.

In all three inhibitor complexes the halogen in position 10 was located at a distance between 3.3 and 3.7 Å from the backbone carbonyl oxygen of the gatekeeper + 3 (gk + 3) Leu241 (Figure 4d). While these distances would be compatible with the formation of halogen bonds, the C–X...O angles (σ -hole angles) of $\sim 135^\circ$ are far from the optimum σ -hole angle which is 180° . For the experimental model of halogen substituted benzenes and *N*-methylacetamide, Wilcken and Boeckler et al. have demonstrated that a deviation of more than 40° from the optimal σ -hole angle leads to virtually complete loss of the complex formation energy.⁶¹ Furthermore, in **5s**, **5t**, and **5j** the distance between the halogen atoms and the carbonyl oxygen of Leu241 is increasing in the order Cl < Br < I. This is contrary to an expected decrease of the distance, which should follow the expected strength of putative halogen bonds. In conclusion, we believe that halogen bond contribution to inhibitor binding is in these cases either nonexistent or very weak. However, the negative belt of a halogen atom, polarized by even very weak halogen bonding, may play a role as hydrogen acceptor motif toward the gk + 3 Leu241 backbone nitrogen. This kind of dual halogen-bond/hydrogen-bond interaction, emanating from a single halogen atom and forming two contacts with the hinge region, was suggested by Wilcken and Boeckler et al.⁶¹ for the inhibitor KH-CB19 with CLK3.³⁹ Along these lines, the inhibitory activity of the 10-methoxy substituted derivative **5k**, which is equipotent to its chloro analogue **5h**, can also be explained. The

methoxy oxygen of **5k** can mimic the hydrogen bond acceptor role of the halogen of **5h**, forming an analogous hydrogen bond to the Leu241 nitrogen.

With double digit nanomolar IC_{50} values measured for DYRK1A, the inhibitors reported here showed comparable potency to other DYRK inhibitors reported in the literature. However, both 10-iodo derivatives **5j** and **5o** showed superior selectivity toward closely related kinases. Because of the potential antagonistic functions of DYRK1 family members, the compounds constitute important chemical tools for further biochemical studies. Comparison of our screening data identified the 10-iodo substituent as the relevant group for the observed selectivity. Although a plausible explanation at a molecular level is not yet available, it is tempting to speculate that only DYRK1A, but not the related protein kinases, is able to accommodate the large 10-iodo substituent of the selective derivatives in the ATP binding pocket.

CONCLUSION

Experimental DYRK1A inhibitors described so far have suffered from poor selectivity toward other closely related protein kinases, namely, other DYRKs and members of the CLK family. We have developed two 10-iodo-11*H*-indolo[3,2-*c*]quinoline-6-carboxylic acids **5j** and **5o** as the first selective inhibitors of DYRK1A. Compound **5j** proved also to inhibit the enzyme in cellular assays. Docking studies and X-ray structure analyses

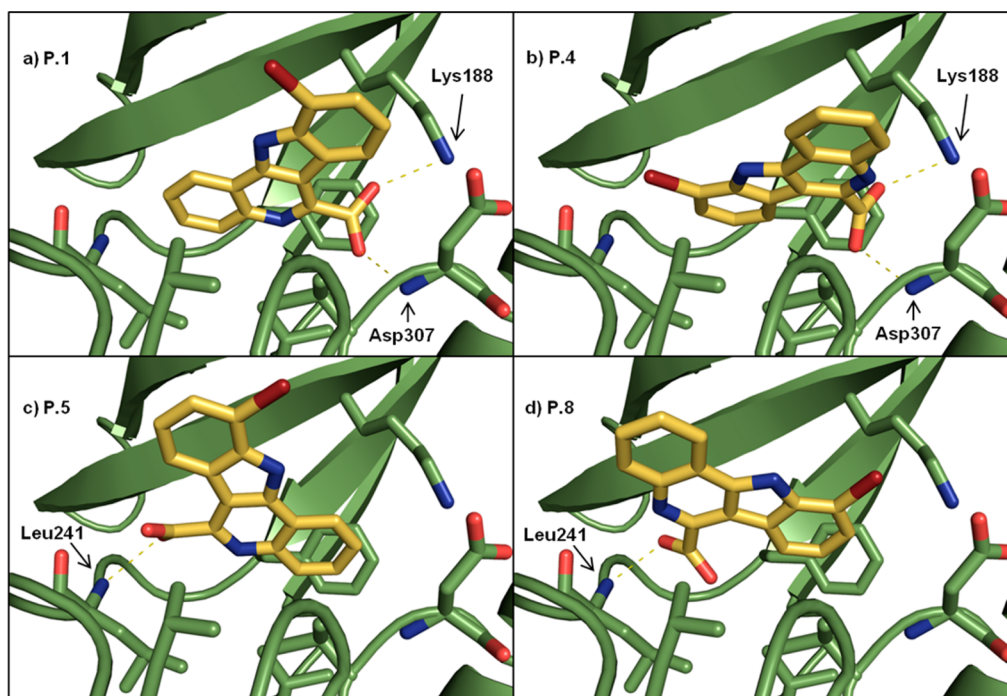


Figure 3. Representative orientations of the 10 highest-ranked docking poses of 5i in the ATP binding site of DYRK1A (template for docking, 2WO6): (a) ranks in the scoring list, 1–3; (b) ranks in the scoring list, 4 and 7; (c) ranks in the scoring list, 5, 6, 10; (d) ranks in the scoring list, 8, 9. P.1 refers to the pose ranked no. 1.

Table 3. Data Collection and Refinement Statistics of Inhibitor–DYRK1A complexes

complex (pdb id)	DYRK1A-5j (4YLJ)	DYRK1A-5s (4YLK)	DYRK1A-5t (4YLL)
	Data Collection		
beamline	Diamond, beamline I04-1	Diamond, beamline I04-1	Diamond, beamline I04-1
wavelength (Å)	0.9200	0.9200	0.9200
resolution ^a (Å)	48.41–2.58 (2.72–2.58)	30.28–1.40 (1.48–1.40)	28.21–1.40 (1.48–1.40)
space group	C 2	C 2	C 2
cell dimensions			
<i>a</i> (Å)	265.5	100.0	100.0
<i>b</i> (Å)	65.5	69.9	69.9
<i>c</i> (Å)	139.4	67.9	67.9
α (deg)	90.0	90.0	90.0
β (deg)	114.6	117.7	117.7
γ (deg)	90.0	90.0	90.0
no. unique reflections ^a	68 848 (10 018)	78 842 (11 510)	77 083 (11 265)
completeness ^a (%)	99.6 (99.9)	97.1 (97.3)	95.0 (95.4)
<i>I</i> / σ <i>I</i> ^a	16.6 (2.2)	10.7 (3.5)	12.4 (4.4)
<i>R</i> _{merge} ^a	0.066 (0.884)	0.077 (0.386)	0.059 (0.268)
redundancy ^a	6.5 (6.6)	4.4 (4.3)	3.3 (3.3)
	Refinement		
no. atoms in refinement (P/L/O) ^b	11 439/164/385	2880/45/647	2849/22/642
<i>R</i> _{fact} (%)	19.2	15.5	15.1
<i>R</i> _{free} (%)	22.2	17.7	17.2
<i>B</i> _f (P/L/O) ^b (Å ²)	79/73/73	13/11/24	13/9/ 23
rmsd bond ^c (Å)	0.011	0.016	0.015
rms deviation angle ^c (deg)	1.4	1.8	1.7
	Molprobit		
Ramachandran favored	96.8	96.3	96.3
Ramachandran allowed	100.0	100.0	100.0

^aValues in brackets show the statistics for the highest resolution shells. ^bP/L/O indicate protein, ligand molecule, and other (water and solvent molecules), respectively. ^crmsd indicates root-mean-square deviation.

revealed a nonclassical binding mode in which inhibitors were oriented via the 10-halogen substituent toward the hinge region

of the kinase. Although the 10-substituent obviously was of central importance for the hinge–inhibitor attraction, the

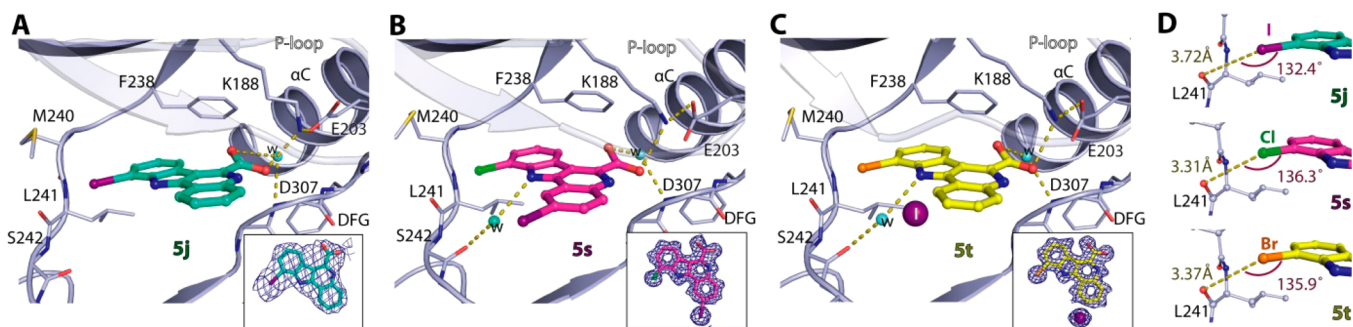


Figure 4. Crystal structure analyses of the binding modes of halogen-substituted DYRK1A inhibitors. Accommodations of three halogen derivatives comprising iodo (**5j**, A), chloro (**5s**, B), and bromo (**5t**, C) substitutions at the position 10 within the ATP pocket share common features of hydrogen bond network interactions (yellow dashed lines) with the kinase. Insets show electron density maps for the bound inhibitors, and water molecules are shown in cyan spheres. (D) Detailed distances and C–X...O angles (putative σ -hole angles) between the halogen groups of the inhibitors and the carbonyl atom of $gk + 3$ Leu241.

nature of this interaction is not yet clear. The title compounds demonstrate that within the CMGC family of protein kinases selective inhibition of DYRK1A is possible. With the aim of developing compounds that are better suited for cellular assays or animal disease models, further studies in this compound class will be directed to increase solubility and cell permeability.

EXPERIMENTAL PROCEDURES

Synthetic Chemistry. Starting materials were purchased from Acros Organics (Geel, Belgium) or Sigma-Aldrich (Steinheim, Germany). Solvents were used as commercially available grades for synthesis, with the exceptions of toluene, THF, CH_2Cl_2 , and diethyl ether, which were dried and purified by published methods.⁶⁵ **5b**, **5c**, and **5f** were prepared as reported previously.⁵⁴ Synthetic procedures and structure characterization data for the following compounds are available in the Supporting Information: **5a**, **5d–e**, **5g–i**, **5k–n**, **5p–w**, **6**, **7**, **10n,s,t**.

Melting points (mp) were determined on an electric variable heater (Electrothermal IA 9100, Barnstedt International, Southend-on-Sea, U.K.) in open glass capillaries. IR spectra were recorded as KBr discs on a Thermo Nicolet FT-IR 200. ¹H NMR spectra and ¹³C NMR spectra were recorded on the following instruments: Bruker Avance DRX-400, Bruker Avance III-400, and Bruker Avance II-600 (Bruker, Billerica, MA, USA); internal standard tetramethylsilane; signals in ppm (δ scale). Signals in ¹³C spectra were assigned based on the results of ¹³C DEPT135 experiments (NMR Laboratories of the Chemical Institutes of the Technische Universität Braunschweig). Elemental analyses were determined on a CE Instruments FlashEA 1112 elemental analyzer (Thermo Quest). Mass spectra were recorded on a Finnigan-MAT 95 (Thermo Finnigan MAT, Bremen, Germany). Accurate measurements were conducted according to the peak match method using perfluorokerosene (PFK) as an internal mass reference. (EI) MS: ionization energy 70 eV (Department of Mass Spectrometry of the Chemical Institutes of the Technische Universität Braunschweig). TLC: Polygram Sil G/UV₂₅₄, Macherey-Nagel, 40 mm × 80 mm, visualization by UV illumination (254 and 366 nm). Purity was determined by HPLC using the following devices and settings. Isocratic elution: Elite LaChrom (Merck/Hitachi), pump L-2130, autosampler L-2200, diode array detector L-2450, organizer box L-2000; column, Merck LiChroCART 1254, LiChrosphere 100, RP 18, 5 μ m; flow rate 1.000 mL/min; volume of injection, 10 μ L; detection (DAD) at 254 and 280 nm; AUC, % method; time of detection 15 min, net retention time (t_N), dead time (t_m) related to DMSO. Gradient elution: Elite LaChrom (Merck/Hitachi), pump L-2130, autosampler L-2200, UV detector L-2400, organizer box L-2000; column, Merck LiChroCART 125-4, LiChrosphere 100, RP 18, 5 μ m; flow rate 1.000 mL/min; volume of injection, 10 μ L; detection at 254 nm; AUC, % method; net retention time (t_N), dead time (t_m) related to DMSO. For all gradient runs, mixtures of ACN and water or aqueous formic or trifluoroacetic acid were used as specified for

particular compounds. Preparation of $H_2O + (Et_3NH)_2SO_4$ buffer (pH 2.6) for isocratic HPLC: triethylamine (20.0 mL) and sodium hydroxide (242 mg) are dissolved in water to 1 L. The solution is adjusted to pH 2.6 by addition of sulfuric acid. All compounds that were biologically tested were of >95% purity with the exception of **5h** (HPLC, 93.6% at 254 nm and 94.8% at 280 nm detection wavelength) and **5w** (HPLC, 95.1% at 254 nm and 94.2% at 280 nm detection wavelength). Absorption maxima (λ_{max}) were extracted from the spectra recorded by the DAD in the HPLC peak maxima in isocratic runs (software, EZ Chrom Elite Client/server, version 3.1.3.).

General Procedure A for the Fischer Indole Synthesis of Paullones 4 Used as Starting Materials for Subsequent Syntheses. An appropriate substituted 3,4-dihydro-1*H*-1-benzazepine-2,5-dione (**1** equiv) and an appropriately substituted phenylhydrazine hydrochloride (1.2–1.5 equiv) and sodium acetate (1.2–1.5 equiv) are stirred in acetic acid (10 mL) at 70 °C for the indicated time. Sulfuric acid (0.1 mL) is added, and stirring at 70 °C is continued for the indicated time. After cooling to room temperature, the mixture is poured into 5% aqueous sodium acetate solution (20 mL) and kept at 8 °C for 2 h. A precipitate is formed, which is filtered off with suction, washed with water and petrol ether. Purification is accomplished by column chromatography or crystallization.

General Procedure B1 for Oxidative Ring Contraction of Paullones 4 To Yield 11*H*-Indolo[3,2-*c*]quinoline-6-carboxylic Acids **5j and **5o**.** The appropriate paullone **4** (1 equiv), NHPI (2 equiv), and cobalt(II) acetate tetrahydrate (0.25 equiv) are dissolved in the given volume of DMF. Oxygen is bubbled through the stirred mixture for the given time at the indicated temperature. The reaction is monitored by TLC. The precipitate is filtered off and washed with water. If no precipitate appears, water (5 mL) is added and the resulting precipitate is separated and purified by centrifugation, decanting, and washing with water. The resulting solid is washed with a small amount of acetone. The predried product is finally dried at 130 °C in vacuo.

General Procedure C for the Syntheses of Ethyl 11*H*-Indolo[3,2-*c*]quinoline-6-carboxylates **10n,o,s,t by Esterification.** Ethanol (100 mL) is added to a solution of an appropriate 11*H*-indolo[3,2-*c*]quinoline-6-carboxylic acid **5** in DMSO (5 mL). Hydrogen chloride gas is bubbled through the solution for 30 min at room temperature. After removal of the ethanol by evaporation, water (100 mL) is added and the mixture is kept at 8 °C for 1 h. The resulting precipitate is filtered off, washed with water, and dissolved in acetone (5 mL). After addition of silica gel (2 g), the mixture is evaporated. The product is subsequently eluted from the silica gel by flash chromatography using the indicated eluent. Finally the product is dried at 100 °C in vacuo.

11-Iodo-7,12-dihydroindolo[3,2-*d*][1]benzazepin-6(5*H*)-one (4j**).** Synthesis was according to general procedure A from 3,4-dihydro-1*H*-1-benzazepine-2,5-dione⁶⁶ (88 mg, 0.50 mmol), 2-iodophenylhydrazine hydrochloride⁶⁶ (203 mg, 0.750 mmol), and sodium acetate (62 mg, 0.75 mmol). Reaction times were 1 h before and 4 h after

addition of sulfuric acid, respectively. Purification by column chromatography (toluene–ethyl acetate–formic acid 5:5:1) yielded a dark yellow powder (51 mg, 28%); mp (dec) starting at 288 °C. IR (KBr): 3194 cm^{-1} (NH), 1666 cm^{-1} (C=O). ^1H NMR (DMSO- d_6 , 400.4 MHz): δ (ppm) = 3.47 (s, 2H), 6.90 (t, 1H, J = 7.6 Hz), 7.22–7.31 (m, 2H), 7.40 (ddd, 1H, J = 7.9/7.4/1.6 Hz), 7.59 (dd, 1H, J = 7.5/0.9 Hz), 7.71 (d, 1H, J = 7.9 Hz), 7.91 (dd, 1H, J = 7.8/1.5 Hz), 10.11 (s, 1H, lactam NH), 11.29 (s, 1H, indole NH). ^{13}C NMR (DMSO- d_6 , 100.7 MHz): δ (ppm) = 31.6 (CH_2); 118.0, 121.1, 122.1, 123.3, 128.3, 128.5, 131.5 (CH); 76.7, 109.4, 122.4, 127.1, 133.6, 135.6, 139.4 (C); 171.7 (C=O). $\text{C}_{16}\text{H}_{11}\text{IN}_2\text{O}$ (374.18). MS (EI): m/z (%) = 374 $[\text{M}]^{+\bullet}$ (100), 373 $[\text{M} - \text{H}]^+$ (35), 345 $[\text{M} - \text{CHO}]^+$ (49). HRMS (EI): m/z $[\text{M}]^{+\bullet}$ calcd 373.99106, found 373.99084. HPLC (isocr): 96.1% at 254 nm and 92.9% at 280 nm, t_{N} = 4.7 min, t_{M} = 1.0 min (ACN/ H_2O 50:50); λ_{max} : 230 and 313 nm.

11-Iodo-3-methoxy-7,12-dihydroindolo[3,2-*d*][1]-benzazepin-6(5*H*)-one (4o). Synthesis was according to general procedure A from 8-methoxy-3,4-dihydro-1*H*-1-benzazepine-2,5-dione^{52,67} (500 mg, 2.44 mmol), 2-iodophenylhydrazine hydrochloride⁵⁶ (993 mg, 3.67 mmol), and sodium acetate (301 mg, 3.67 mmol). Reaction times were 3 h before and 16 h after addition of sulfuric acid, respectively. Purification by column chromatography (toluene–ethyl acetate–formic acid 5:5:1) yielded a dark yellow powder (340 mg, 34%); mp (dec) starting at 290 °C. IR (KBr): 3205 cm^{-1} (NH), 1680 cm^{-1} (C=O). ^1H NMR (DMSO- d_6 , 600.1 MHz): δ (ppm) = 3.47 (s, 2H), 3.81 (s, 3H), 6.82 (d, 1H, J = 2.6 Hz), 6.88 (t, 1H, J = 7.7 Hz), 6.91 (dd, 1H, J = 8.7/2.6 Hz), 7.55 (dd, 1H, J = 7.5/0.9 Hz), 7.67 (d, 1H, J = 7.8 Hz), 7.85 (d, 1H, J = 8.7 Hz), 10.04 (s, 1H, lactam NH), 11.19 (s, 1H, indole NH). ^{13}C NMR (DMSO- d_6 , 150.9 MHz): δ (ppm) = 55.2 (CH_3), 31.6 (CH_2), 106.6, 109.9, 117.6, 121.0, 129.6, 130.9 (CH), 76.5 (C(11)), 107.6, 115.3, 127.1, 133.8, 136.9, 139.0, 159.2 (C). 171.3 (C=O). $\text{C}_{17}\text{H}_{13}\text{IN}_2\text{O}_2$ (404.20); calcd C 50.51, H 3.24, N 6.93, found C 50.38, H 3.29, N 6.72. MS (EI): m/z (%) = 404 $[\text{M}]^{+\bullet}$ (100), 403 $[\text{M} - \text{H}]^+$ (36), 375 $[\text{M} - \text{CHO}]^+$ (42). HRMS (EI): m/z $[\text{M}]^{+\bullet}$ calcd 404.00162, found 404.00161. HPLC (isocr): 96.0% at 254 nm and 95.2% at 280 nm, t_{N} = 5.2 min, t_{M} = 1.0 min (ACN/ H_2O 50:50). λ_{max} : 234 and 313 nm.

10-Iodo-11*H*-indolo[3,2-*c*]quinoline-6-carboxylic Acid (5j). Synthesis was according to general procedure B1 from 11-iodo-7,12-dihydroindolo[3,2-*d*][1]benzazepin-6(5*H*)-one (4j, 43 mg, 0.11 mmol), NHPI (36 mg, 0.22 mmol), and cobalt(II) acetate tetrahydrate (7 mg, 0.03 mmol) in DMF (2 mL). Oxygen was bubbled through the reaction mixture at room temperature for 4 h. A yellow powder was formed, which was purified by washing with acetone (34 mg, 82%); mp (dec) 358–359 °C. IR (KBr): 3224 cm^{-1} (NH), 1659 cm^{-1} (C=O). ^1H NMR (DMSO- d_6 , 400.4 MHz): δ (ppm) = 7.10 (t, 1H, J = 7.7 Hz), 7.35–7.42 (m, 1H), 7.56–7.62 (m, 2H), 7.82 (dd, 1H, J = 7.7/1.0 Hz), 8.30 (dd, 1H, J = 8.0/1.0 Hz), 8.38 (d, 1H, J = 8.0 Hz), 11.54 (s, 1H, NH), 11.95 (s, 1H, COOH). ^{13}C NMR (DMSO- d_6 , 100.7 MHz): δ (ppm) = 121.2 (2C), 123.4, 124.4, 129.2, 131.1, 134.8 (CH); 76.7 (C(10)), 115.5, 117.2, 127.3, 135.2, 139.3, 142.5, 161.8 (C); 176.3 (C=O). $\text{C}_{16}\text{H}_9\text{IN}_2\text{O}_2$ (388.16). MS (EI): m/z (%) = 388 $[\text{M}]^{+\bullet}$ (37), 360 $[\text{M} - \text{CO}]^{+\bullet}$ (100). HRMS (EI): m/z $[\text{M}]^{+\bullet}$ calcd 387.97032, found 387.96899. HPLC (isocr): 96.7% at 254 nm and 98.6% at 280 nm, t_{N} = 2.8 min, t_{M} = 1.0 min (ACN/ H_2O + (Et_3N)₂SO₄ 50:50). λ_{max} : 238, 280, and 307 nm. HPLC (grad): 97.4% at 254 nm, t_{N} = 10.0 min, t_{M} = 1.1 min (ACN/ H_2O ; 0 min, 10/90 → 13 min, 90/10 (linear); 20 min, 90/10).

10-Iodo-3-methoxy-11*H*-indolo[3,2-*c*]quinoline-6-carboxylic Acid (5o). Synthesis was according to general procedure B1 from 11-iodo-3-methoxy-7,12-dihydroindolo[3,2-*d*][1]benzazepin-6(5*H*)-one (4o, 40 mg, 0.10 mmol), NHPI (33 mg, 0.20 mmol), and cobalt(II) acetate tetrahydrate (7 mg, 0.03 mmol) in DMF (2 mL). Oxygen was bubbled through the reaction mixture for 1 h. For the purification by column chromatography, impurities were removed initially by elution with toluene–ethyl acetate–diethylamine (1:1:1) prior to elution by toluene–ethyl acetate–formic acid 2:2:1. Yellow powder (20 mg, 48%); mp (dec) 346–348 °C. IR (KBr): 3200 cm^{-1} (NH), 1669 cm^{-1} (C=O). ^1H NMR (DMSO- d_6 , 600.1 MHz): δ (ppm) = 3.86 (s, 3H), 7.01 (dd, 1H, J = 9.0/2.6 Hz), 7.07 (t, 1H, J = 7.7 Hz), 7.17 (d, 1H, J =

2.5 Hz), 7.78 (dd, 1H, J = 7.5/0.9 Hz), 8.31 (dd, 1H, J = 7.9/0.7 Hz), 8.36 (d, 1H, J = 9.0 Hz), 11.44 (s, 1H, NH), 11.76 (s, 1H, COOH). ^{13}C NMR (DMSO- d_6 , 150.9 MHz): δ (ppm) = 55.5 (CH_3); 104.9, 110.6, 121.1, 124.2, 130.8, 134.4 (CH_2); 76.3, 110.3, 114.2, 127.5, 137.0, 139.1, 143.0, 161.1, 161.5 (C); 175.5 (C=O). $\text{C}_{17}\text{H}_{11}\text{IN}_2\text{O}_3$ (418.19). MS (EI): m/z (%) = 418 $[\text{M}]^{+\bullet}$ (47), 390 $[\text{M} - \text{CO}]^{+\bullet}$ (100), 375 $[\text{M} - 43]^+$ (24), 347 $[\text{M} - 71]^+$ (22). HRMS (EI): m/z $[\text{M}]^{+\bullet}$ calcd 417.98089, found 417.98126. HPLC (isocr): 96.3% at 254 nm and 97.7% at 280 nm, t_{N} = 3.2 min, t_{M} = 1.0 min (ACN/ H_2O + (Et_3N)₂SO₄ 50:50). λ_{max} : 247, 306, and 375 nm. HPLC (grad): 99.4% at 254 nm, t_{N} = 10.8 min, t_{M} = 1.2 min (gradient, ACN/ H_2O ; 0 min, 10/90 → 13 min, 90/10 (linear); 20 min, 90/10).

Ethyl 10-iodo-3-methoxy-11*H*-indolo[3,2-*c*]quinoline-6-carboxylate (10o). Synthesis was according to general procedure C from 10-iodo-3-methoxy-11*H*-indolo[3,2-*c*]quinoline-6-carboxylic acid (5o, 120 mg, 0.300 mmol). Purification by column chromatography (toluene–ethyl acetate–diethylamine 2:2:1) yielded pale yellow crystals (100 mg, 75%); mp 214–217 °C. IR (KBr): 3384 (NH), 1726 cm^{-1} (C=O). ^1H NMR (DMSO- d_6 , 400.4 MHz): δ (ppm) = 1.45 (t, 3H, J = 7.1 Hz), 3.99 (s, 3H), 4.59 (q, 2H, J = 7.1 Hz), 7.14 (t, 1H, J = 7.8 Hz), 7.46 (dd, 1H, J = 9.1/2.6 Hz), 7.63 (d, 1H, J = 2.6 Hz), 7.93 (dd, 1H, J = 7.6/1.0 Hz), 8.33 (dd, 1H, J = 8.1/0.9 Hz), 9.05 (d, 1H, J = 9.1 Hz), 12.34 (s, 1H, NH). ^{13}C NMR (DMSO- d_6 , 100.7 MHz): δ (ppm) = 14.2 (CH_2 – CH_3); 55.5 (OCH₃); 61.7 (CH_2); 108.7, 119.1, 122.0, 122.5, 124.7, 135.1 (CH); 76.8, 111.2, 111.8, 121.4, 141.1, 142.0, 145.1, 146.0, 160.1 (C); 166.7 (C=O). $\text{C}_{19}\text{H}_{15}\text{IN}_2\text{O}_3$ (446.24); calcd C 51.14, H 3.39, N 6.28, found C 51.21, H 3.41, N 6.01. MS (EI): m/z (%) = 446 $[\text{M}]^{+\bullet}$ (22), 374 $[\text{M} - \text{C}_3\text{H}_4\text{O}_2]^+$ (100). HPLC (isocr): 99.7% at 254 nm and 99.8% at 280 nm, t_{N} = 7.6 min, t_{M} = 1.0 min (ACN/ H_2O 80:20). λ_{max} : 243 and 286 nm. HPLC (grad): 99.7% at 254 nm, t_{N} = 14.1 min, t_{M} = 1.1 min (gradient, ACN/ H_2O ; 0 min, 10/90 → 13 min, 90/10 (linear); 20 min, 90/10). Crystals for X-ray structure analysis were prepared by crystallization from ethanol (96%).

X-ray Crystal Structure Analysis of 10o. Crystal data for 10o- H_2O at 100 K: orthorhombic, $P2_12_12_1$, a = 6.36362(12), b = 15.0401(3), c = 18.3209(4) Å, V = 1753.48 Å³, Z = 4. A yellow irregular crystal 0.3 mm × 0.2 mm × 0.15 mm was used to record 76097 intensities, 5096 independent (R_{int} = 0.036) on an Oxford Diffraction Xcalibur E diffractometer using Mo $K\alpha$ radiation (λ = 0.71073 Å, $2\theta_{\text{max}}$ = 60°). The structure was refined anisotropically on F^2 using the program SHELXL-97 to $wR2$ = 0.049, $R1$ = 0.020 for 249 parameters; S = 1.12, max. $\Delta\rho$ = 1.4 e Å⁻³. Crystallographic data have been deposited with the Cambridge Crystallographic Data Centre as supplementary publication no. CCDC-1036693. Copies of the data can be obtained free of charge from www.ccdc.cam.ac.uk/data_request/cif.

Kinase Expression and Activity Assays. Protein Kinase Assays. Buffer A consisted of 10 mM MgCl₂, 1 mM EGTA, 1 mM DTT, 25 mM Tris-HCl, pH 7.5, 50 μg heparin/mL. Buffer C consisted of 60 mM β-glycerophosphate, 15 mM *p*-nitrophenylphosphate, 25 mM MOPS (pH 7.2), 15 mM EGTA, 15 mM MgCl₂, 1 mM DTT, 1 mM sodium vanadate, 1 mM phenylphosphate.

Kinase activities were assayed in buffer A or C at 30 °C at a final ATP concentration of 15 μmol/L. Blank values were subtracted, and activities were expressed in percent of the maximal activity, i.e., in the absence of inhibitors. Controls were performed with appropriate dilutions of DMSO. The GS-1, CKS, CDK7/9 tide, and RS peptide substrates were obtained from Proteogenix (Oberhausbergen, France).

CDK1/cyclin B (M phase starfish oocytes, native), CDK2/cyclin A, and CDK5/p25 (human, recombinant) were prepared as previously described.⁶⁸ Their kinase activity was assayed in buffer A, with 1 mg of histone H1/mL, in the presence of 15 μmol/L [γ -33P] ATP (3000 Ci/mmol; 10 mCi/mL) in a final volume of 30 μL. After a 30 min incubation at 30 °C, the reaction was stopped by harvesting onto P81 phosphocellulose supernatant (Whatman) using a FilterMate harvester (Packard) and washing in 1% phosphoric acid. Scintillation fluid was added and the radioactivity measured in a Packard counter.

CDK9/cyclin T (human, recombinant, expressed in insect cells) was assayed as described for CDK1/cyclin B but using CDK7/9 tide (YSPTSPSYSPSPSYSPSPSKKKK) (8.1 $\mu\text{g}/\text{assay}$) as a substrate.

GSK-3 (porcine brain, native, affinity purified on axin1-Sepharose beads) was assayed, as described for CDK1, with 0.5 mg of BSA/mL + 1 mM DTT and using a GSK-3 specific substrate (GS-1, YRRAAVPPSPSLSRHSSPHQSpEDEEE) (pS stands for phosphorylated serine).⁶⁹

CK1 δ/ϵ (porcine brain, native, affinity purified on axin2-Sepharose beads) was assayed as described for CDK1 but in buffer C and using 25 μM CKS peptide (RRKHAAIGpSAYSITA), a CK1-specific substrate.⁷⁰

CLK1, -2, -3, and -4 (mouse, recombinant, expressed in *E. coli* as GST fusion proteins) were assayed as described for CDK1/cyclin B with 0.5 mg BSA/mL + 1 mM DTT and RS peptide (GRSRS-RSRSRSR) (1 $\mu\text{g}/\text{assay}$) as a substrate.

DYRK1A, -1B, -2, -3 (human, recombinant, expressed in *E. coli* as GST fusion proteins) and CLK1, -2, -3, and -4 (mouse, recombinant, expressed in *E. coli* as GST fusion proteins) were assayed in buffer A (supplemented extemporaneously with 0.15 mg of BSA/mL + 1 mM DTT) with 1 μg of RS peptide (GRSRSRSRSRSR) as a substrate.

All data points for construction of dose–response curves were recorded in triplicate. Typically, the standard deviation of single data points was below 10%.

Inhibition of Cellular DYRK1A Activity. The assay for inhibition of SF3B1 phosphorylation was performed as described previously.⁵⁸ For the assay of tau phosphorylation, we used a HEK293 subclone with regulatable expression of GFP-DYRK1A and constitutive expression of GFP-tau (HEK293-tau-DYRK1A) that was kindly provided by Dr. Matthias Engel (Department of Pharmaceutical and Medicinal Chemistry, Saarland University, Saarbrücken, Germany).⁵⁹ Cells were grown overnight in six-well plates before expression of GFP-DYRK1A was induced with 2 $\mu\text{g}/\text{mL}$ doxycyclin. The inhibitors were then added from stock solutions in DMSO to the desired final concentration and cells were further incubated for 20 h. Cells were lysed in SDS lysis buffer (20 mM Tris-HCl, pH 7.4, 1% SDS). Samples were sonicated and cleared by centrifugation before SDS–PAGE and immunoblotting with a goat antibody for GFP (no. 600-101-215, Rockland Immunochemicals, Gilbertsville, PA, USA) and a phosphorylation state specific antibody directed against pThr212 in the tau protein (no. 44740G, Invitrogen, Camarillo, CA, USA). Immunoreactivities were detected by enhanced chemiluminescence using HRP-coupled secondary antibodies and quantified using the AIDA Image Analyzer 5.0 program (Raytest, Straubenhardt, Germany). Relative tau phosphorylation was calculated by normalization to total tau expression, as determined from GFP immunoreactivity. To calculate relative DYRK1A activity, the basal pT212 signal in control cells not treated with doxycyclin was subtracted from all values, and the phosphorylation in DYRK1A expressing cells not treated with inhibitors was set to 100%. Curve fitting for IC₅₀ determination was done with the help of the GraphPad Prism 5.0 program (GraphPad Software, La Jolla, CA, USA).

Crystallography and Molecular Modeling. Protein Production, Crystallization of DYRK1A–Inhibitor Complexes, Data Collection, and Structure Determination. Recombinant DYRK1A was purified as previously described⁶⁰ and was treated with TEV protease to remove the N-terminal His₆ tag. The kinase at ~13–15 mg/mL in 50 mM HEPES, pH 7.5, 500 mM NaCl and 5 mM DTT was incubated with the inhibitors at 1 mM prior to crystallization. Crystals were obtained using the sitting drop vapor diffusion method at 4 °C using either 2 M ammonium sulfate, 0.2 M Na/K tartrate, 0.1 M citrate, pH 5.6 (for 5s and 5t), or 37% PEG 400, 0.2 M lithium sulfate, 0.1 M Tris, pH 8.8 (for 5j), as the reservoir solutions. Diffraction data collected at Diamond Light Source, beamline I04-1, were processed with XDS⁷¹ or mosflm⁷² and subsequently scaled with Scala from CCP4 suite.⁷³ Structures were determined by molecular replacement method using Phaser⁷⁴ and the coordinates of DYRK1A structure⁶⁰ as a search model. Iterative cycles of manual model building in COOT⁷⁵ alternated with refinement using Refmac,⁷⁶ and a TLS model calculated from TLSMD server⁷⁷ was performed. The

geometric correctness of the final model was verified with MolProbity.⁷⁸ Data collection and refinement statistics are summarized in Table 3. DYRK1A–ligand complexes (pdb id): DYRK1A-5j (4YLJ); DYRK1A-5s (4YLK); DYRK1A-5t (4YLL).

Docking. Molecular docking was performed using GOLD,⁷⁹ version 4.0, running under Linux Ubuntu Dapper Drake. The poses obtained with GOLD 4.0 were later reproduced using GOLD, version 5.1. The PDB file 2WO6 was downloaded from the Protein Data Bank. Only the B chain present in the structure was used for docking. The wizard integrated in GOLD was used for loading the structure into the user interface HERMES. Hydrogen atoms were added, and the protonation/tautomerization status of amino acid side chains within the ATP binding site was checked and adjusted manually, if necessary. Ligand and water molecules were deleted from the structure. A zone of 10 Å around the original ligand was defined as relevant for binding. The options “flip side chains of Asn/Gln” and “alter tautomers of His” were switched off. Ligands were constructed with MOE,⁸⁰ energy minimized, and saved as mol2 files. The option “save lone pairs” was switched off and “search efficiency” was set to 200%. Ten GA runs were performed without constraints and “allow early termination” option switched off. Scoring of resulting poses was performed applying the integrated chemscore.kinase template. Redocking of the originally bound ligand DJM2005 into chain B of the protein reproduced the original pose of the inhibitor, albeit not as highest ranked pose.

■ ASSOCIATED CONTENT

📄 Supporting Information

Details for the crystal structure analysis of compound **10o** as well as synthesis and spectroscopic data of compounds **5a,b,d,e,g–i,k–n,p–w**, **6**, **7**, and **10n,s,t** and HPLC purity data of all compounds employed in biological tests. This material is available free of charge via the Internet at <http://pubs.acs.org>.

■ AUTHOR INFORMATION

Corresponding Authors

*L.M., for biology: e-mail, meijer@manros-therapeutics.com; phone, +33-608605834.

*C.K., for chemistry: e-mail, c.kunick@tu-braunschweig.de; phone, +49-5313912754; fax, +49-5313912799.

Notes

The authors declare no competing financial interest.

■ ACKNOWLEDGMENTS

This research was supported by grants from the “Fonds Unique Interministériel” (FUI) TRIAD Project (L.M.), the “Association France-Alzheimer (Finistère)” (L.M.), the “Fondation Jérôme Lejeune” (L.M.), the German Research Foundation (DFG Grant Be 1967/3-1 to W.B.), and Grant FP7-KBBE-2012 (BlueGenics) (L.M.). S.K. receives funding from the SGC, a registered charity (No. 1097737) that receives funds from AbbVie, Bayer Pharma AG, Boehringer Ingelheim, the Canada Foundation for Innovation, Genome Canada, Glaxo-SmithKline, Janssen, Lilly Canada, the Novartis Research Foundation, the Ontario Ministry of Economic Development and Innovation, Pfizer, Takeda, and the Wellcome Trust [Grant 092809/Z/10/Z]. A.C. is supported by the European Union FP7 Grant 278568 “PRIMES” (Protein Interaction Machines in Oncogenic EGF Receptor Signaling). We thank Sophie Kaspar for performing cell-based assays and Dr. Matthias Engel (Saarland University, Saarbrücken, Germany) for providing the HEK293-tau-DYRK1A cell line.

■ ABBREVIATIONS USED

ACN, acetonitrile; AD, Alzheimer's disease; CDK, cyclin-dependent protein kinase; CK, casein kinase; CLK, cdc2-like kinase; DAD, diode array detector; DANDY, 3,5-diaryl-7-azaindole; dec, decomposition; DH, DYRK homology; DTT, dithiothreitol; DMF, *N,N*-dimethylformamide; DSCR, Down syndrome critical region; DYRK1A, dual-specificity tyrosine phosphorylation-regulated kinase 1A; EGCG, epigallocatechin 3-gallate; EGTA, ethylene glycol tetraacetic acid; ERK, extracellular-signal regulated kinase; GA, genetic algorithm; GFP, green fluorescent protein; gk, gatekeeper; grad, gradient; GSK-3, glycogen synthase kinase 3; GST, glutathione S-transferase; HEPES, *N*-2-hydroxyethylpiperazine-*N'*-2-ethanesulfonic acid; isocr, isocratic; LB, Luria-Bertani; MAO A, monoamine oxidase A; MAP, mitogen-activated protein; MES, 2-(*N*-morpholino)ethanesulfonic acid; MOPS, 3-(*N*-morpholino)propanesulfonic acid; NHPI, *N*-hydroxyphthalimide; PIM1, protein kinase encoded by the proto-oncogene PIM1; PFK, perfluorokerosene; TEV, tobacco etch virus; TLC, thin layer chromatography

■ REFERENCES

- (1) Lejeune, J.; Gautier, M.; Turpin, R. Study of somatic chromosomes from 9 mongoloid children. *C. R. Hebd. Seances Acad. Sci.* **1959**, *248*, 1721–1722.
- (2) Rachidi, M.; Lopes, C. Mental retardation and associated neurological dysfunctions in Down syndrome: a consequence of dysregulation in critical chromosome 21 genes and associated molecular pathways. *Eur. J. Paediatr. Neurol.* **2008**, *12*, 168–182.
- (3) Korenberg, J. R.; Kawashima, H.; Pulst, S. M.; Ikeuchi, T.; Ogasawara, N.; Yamamoto, K.; Schonberg, S. A.; West, R.; Allen, L.; Magenis, E.; Ikawa, K.; Taniguchi, N.; Epstein, C. J. Molecular definition of a region of chromosome 21 that causes features of the Down syndrome phenotype. *Am. J. Hum. Genet.* **1990**, *47*, 236–246.
- (4) McCormick, M. K.; Schinzel, A.; Petersen, M. B.; Stetten, G.; Driscoll, D. J.; Cantu, E. S.; Tranebjaerg, L.; Mikkelsen, M.; Watkins, P. C.; Antonarakis, S. E. Molecular genetic approach to the characterization of the “Down syndrome region” of chromosome 21. *Genomics* **1989**, *5*, 325–331.
- (5) Rahmani, Z.; Bloui, J. L.; Creau-Goldberg, N.; Watkins, P. C.; Mattei, J. F.; Poissonnier, M.; Prieur, M.; Chettouh, Z.; Nicole, A.; Aurias, A.; Sinet, P.-M.; Delabar, J.-M. Critical role of the D21S55 region on chromosome 21 in the pathogenesis of Down syndrome. *Proc. Natl. Acad. Sci. U.S.A.* **1989**, *86*, 5958–5962.
- (6) Park, J.; Song, W.; Chung, K. Function and regulation of Dyrk1A: towards understanding Down syndrome. *Cell. Mol. Life Sci.* **2009**, *66*, 3235–3240.
- (7) Tejedor, F. J.; Hämmerle, B. MNB/DYRK1A as a multiple regulator of neuronal development. *FEBS J.* **2011**, *278*, 223–235.
- (8) Wegiel, J.; Gong, C. X.; Hwang, Y. W. The role of DYRK1A in neurodegenerative diseases. *FEBS J.* **2011**, *278*, 236–245.
- (9) Savage, M. J.; Gingrich, D. E. Advances in the development of kinase inhibitor therapeutics for Alzheimer's disease. *Drug Dev. Res.* **2009**, *70*, 125–144.
- (10) Kimura, R.; Kamino, K.; Yamamoto, M.; Nuripa, A.; Kida, T.; Kazui, H.; Hashimoto, R.; Tanaka, T.; Kudo, T.; Yamagata, H.; Tabara, Y.; Miki, T.; Akatsu, H.; Kosaka, K.; Funakoshi, E.; Nishitomi, K.; Sakaguchi, G.; Kato, A.; Hattori, H.; Uema, T.; Takeda, M. The DYRK1A gene, encoded in chromosome 21 Down syndrome critical region, bridges between beta-amyloid production and tau phosphorylation in Alzheimer disease. *Hum. Mol. Genet.* **2007**, *16*, 15–23.
- (11) Ryoo, S. R.; Jeong, H. K.; Radnaabazar, C.; Yoo, J. J.; Cho, H. J.; Lee, H. W.; Kim, I. S.; Cheon, Y. H.; Ahn, Y. S.; Chung, S. H.; Song, W. J. DYRK1A-mediated hyperphosphorylation of Tau. A functional link between Down syndrome and Alzheimer disease. *J. Biol. Chem.* **2007**, *282*, 34850–34857.
- (12) Shi, J.; Zhang, T.; Zhou, C.; Choha, M. O.; Gu, X.; Wegiel, J.; Zhou, J.; Hwang, Y. W.; Iqbal, K.; Grundke-Iqbal, I.; Gong, C. X.; Liu, F. Increased dosage of Dyrk1A alters alternative splicing factor (ASF)-regulated alternative splicing of tau in Down syndrome. *J. Biol. Chem.* **2008**, *283*, 28660–28669.
- (13) Toiber, D.; Azkona, G.; Ben-Ari, S.; Torán, N.; Soreq, H.; Dierssen, M. Engineering DYRK1A overdosage yields Down syndrome-characteristic cortical splicing aberrations. *Neurobiol. Dis.* **2010**, *40*, 348–359.
- (14) Ryoo, S. R.; Cho, H. J.; Lee, H. W.; Jeong, H. K.; Radnaabazar, C.; Kim, Y. S.; Kim, M. J.; Son, M. Y.; Seo, H.; Chung, S. H.; Song, W. J. Dual-specificity tyrosine(Y)-phosphorylation regulated kinase 1A-mediated phosphorylation of amyloid precursor protein: evidence for a functional link between Down syndrome and Alzheimer's disease. *J. Neurochem.* **2008**, *104*, 1333–1344.
- (15) Ryu, Y. S.; Park, S. Y.; Jung, M. S.; Yoon, S. H.; Kwen, M. Y.; Lee, S. Y.; Choi, S. H.; Radnaabazar, C.; Kim, M. K.; Kim, H.; Kim, K.; Song, W. J.; Chung, S. H. Dyrk1A-mediated phosphorylation of presenilin 1: a functional link between Down syndrome and Alzheimer's disease. *J. Neurochem.* **2010**, *115*, 574–584.
- (16) Becker, W.; Joost, H. G. Structural and functional characteristics of Dyrk, a novel subfamily of protein kinases with dual specificity. *Prog. Nucleic Acid Res. Mol. Biol.* **1999**, *62*, 1–17.
- (17) Himpel, S.; Panzer, P.; Eirimbter, K.; Czajkowska, H.; Sayed, M.; Packman, L. C.; Blundell, T.; Kentrup, H.; Grötzinger, J.; Joost, H. G.; Becker, W. Identification of the autophosphorylation sites and characterization of their effects in the protein kinase DYRK1A. *Biochem. J.* **2001**, *359*, 497–505.
- (18) Kentrup, H.; Becker, W.; Heukelbach, J.; Wilmes, A.; Schürmann, A.; Huppertz, C.; Kainulainen, H.; Joost, H. G. Dyrk, a dual specificity protein kinase with unique structural features whose activity is dependent on tyrosine residues between subdomains VII and VIII. *J. Biol. Chem.* **1996**, *271*, 3488–3495.
- (19) Becker, W.; Sippl, W. Activation, regulation, and inhibition of DYRK1A. *FEBS J.* **2011**, *278*, 246–256.
- (20) Becker, W.; Soppa, U.; Tejedor, F. J. DYRK1A: a potential drug target for multiple Down syndrome neuropathologies. *CNS Neurol. Disord.: Drug Targets* **2014**, *13*, 26–33.
- (21) Karaman, M. W.; Herrgard, S.; Treiber, D. K.; Gallant, P.; Atteridge, C. E.; Campbell, B. T.; Chan, K. W.; Ciceri, P.; Davis, M. I.; Edeen, P. T.; Faraoni, R.; Floyd, M.; Hunt, J. P.; Lockhart, D. J.; Milanov, Z. V.; Morrison, M. J.; Pallares, G.; Patel, H. K.; Pritchard, S.; Wodicka, L. M.; Zarrinkar, P. P. A quantitative analysis of kinase inhibitor selectivity. *Nat. Biotechnol.* **2008**, *26*, 127–132.
- (22) Davis, M. I.; Hunt, J. P.; Herrgard, S.; Ciceri, P.; Wodicka, L. M.; Pallares, G.; Hocker, M.; Treiber, D. K.; Zarrinkar, P. P. Comprehensive analysis of kinase inhibitor selectivity. *Nat. Biotechnol.* **2011**, *29*, 1046–1051.
- (23) Hanks, S. K.; Hunter, T. Protein kinases 6. The eukaryotic protein kinase superfamily: kinase (catalytic) domain structure and classification. *FASEB J.* **1995**, *9*, 576–596.
- (24) Smith, B.; Medda, F.; Gokhale, V.; Dunckley, T.; Hulme, C. Recent advances in the design, synthesis, and biological evaluation of selective DYRK1A inhibitors: a new avenue for a disease modifying treatment of Alzheimer's? *ACS Chem. Neurosci.* **2012**, *3*, 857–872.
- (25) Airaksinen, M. M.; Lecklin, A.; Saano, V.; Tuomisto, L.; Gynther, J. Tremorogenic effect and inhibition of tryptamine and serotonin receptor binding by beta-carbolines. *Pharmacol. Toxicol.* **1987**, *60*, 5–8.
- (26) Kim, H.; Sablin, S. O.; Ramsay, R. R. Inhibition of monoamine oxidase A by beta-carboline derivatives. *Arch. Biochem. Biophys.* **1997**, *337*, 137–142.
- (27) Ogawa, Y.; Nonaka, Y.; Goto, T.; Ohnishi, E.; Hiramoto, T.; Kii, I.; Yoshida, M.; Ikura, T.; Onogi, H.; Shibuya, H.; Hosoya, T.; Ito, N.; Hagiwara, M. Development of a novel selective inhibitor of the Down syndrome-related kinase Dyrk1A. *Nat. Commun.* **2010**, *1*, 86.
- (28) Bain, J.; McLauchlan, H.; Elliott, M.; Cohen, P. The specificities of protein kinase inhibitors: an update. *Biochem. J.* **2003**, *371*, 199–204.

- (29) Adayev, T.; Chen-Hwang, M. C.; Murakami, N.; Wegiel, J.; Hwang, Y. W. Kinetic properties of a MNB/DYRK1A mutant suitable for the elucidation of biochemical pathways. *Biochemistry* **2006**, *45*, 12011–12019.
- (30) Khan, N.; Afaq, F.; Saleem, M.; Ahmad, N.; Mukhtar, H. Targeting multiple signaling pathways by green tea polyphenol (–)-epigallocatechin-3-gallate. *Cancer Res.* **2006**, *66*, 2500–2505.
- (31) Debdab, M.; Carreaux, F.; Renault, S.; Soundararajan, M.; Fedorov, O.; Filippakopoulos, P.; Lozach, O.; Babault, L.; Tahtouh, T.; Baratte, B.; Ogawa, Y.; Hagiwara, M.; Eisenreich, A.; Rauch, U.; Knapp, S.; Meijer, L.; Bazureau, J. P. Leucettines, a class of potent inhibitors of cdc2-like kinases and dual specificity, tyrosine phosphorylation regulated kinases derived from the marine sponge leucettamine B: modulation of alternative pre-RNA splicing. *J. Med. Chem.* **2011**, *54*, 4172–4186.
- (32) Fant, X.; Durieu, E.; Chicanne, G.; Payrastré, B.; Sbrissa, D.; Shisheva, A.; Limanton, E.; Carreaux, F.; Bazureau, J. P.; Meijer, L. Cdc-like/dual-specificity tyrosine phosphorylation-regulated kinases leucettine L41 induces mTOR-dependent autophagy: implication for Alzheimer's disease. *Mol. Pharmacol.* **2014**, *85*, 441–450.
- (33) Tahtouh, T.; Elkins, J. M.; Filippakopoulos, P.; Soundararajan, M.; Burgy, G.; Durieu, E.; Cochet, C.; Schmid, R. S.; Lo, D. C.; Delhomme, F.; Oberholzer, A. E.; Pearl, L. H.; Carreaux, F.; Bazureau, J. P.; Knapp, S.; Meijer, L. Selectivity, cocrystal structures and neuroprotective properties of leucettines, a family of protein kinase inhibitors derived from the marine sponge alkaloid leucettamine B. *J. Med. Chem.* **2012**, *55*, 9312–9330.
- (34) Giraud, F.; Alves, G.; Debiton, E.; Nauton, L.; Théry, V.; Durieu, E.; Ferandin, Y.; Lozach, O.; Meijer, L.; Anizon, F.; Pereira, E.; Moreau, P. Synthesis, protein kinase inhibitory potencies, and in vitro antiproliferative activities of meridianin derivatives. *J. Med. Chem.* **2011**, *54*, 4474–4489.
- (35) Myrianthopoulos, V.; Kritsanida, M.; Gaboriaud-Kolar, N.; Magiatis, P.; Ferandin, Y.; Durieu, E.; Lozach, O.; Cappel, D.; Soundararajan, M.; Filippakopoulos, P.; Sherman, W.; Knapp, S.; Meijer, L.; Mikros, E.; Skaltsounis, A. L. Novel inverse binding mode of indirubin derivatives yields improved selectivity for DYRK kinases. *ACS Med. Chem. Lett.* **2013**, *4*, 22–26.
- (36) Leblond, B.; Casagrande, A.-S.; Désiré, L.; Foucourt, A.; Besson, T. Tricyclic pyrimidines as inhibitors of DYRK1A/DYRK1B as potential treatment for Down's syndrome or Alzheimer's disease. *WO 2013/026806A1*, 2013.
- (37) Anderson, K.; Chen, Y.; Chen, Z.; Dominique, R.; Glenn, K.; He, Y.; Janson, C.; Luk, K. C.; Lukacs, C.; Polonskaia, A.; Qiao, Q.; Railkar, A.; Rossman, P.; Sun, H.; Xiang, Q.; Vilenchik, M.; Wovkulich, P.; Zhang, X. Pyrido[2,3-*d*]pyrimidines: discovery and preliminary SAR of a novel series of DYRK1B and DYRK1A inhibitors. *Bioorg. Med. Chem. Lett.* **2013**, *23*, 6610–6615.
- (38) Gourdain, S.; Dairou, J.; Denhez, C.; Bui, L. C.; Rodrigues-Lima, F.; Janel, N.; Delabar, J. M.; Cariou, K.; Dodd, R. H. Development of DANDYs, new 3,5-diaryl-7-azaindoles demonstrating potent DYRK1A kinase inhibitory activity. *J. Med. Chem.* **2013**, *56*, 9569–9585.
- (39) Fedorov, O.; Huber, K.; Eisenreich, A.; Filippakopoulos, P.; King, O.; Bullock, A. N.; Szklarczyk, D.; Jensen, L. J.; Fabbro, D.; Trappe, J.; Rauch, U.; Bracher, F.; Knapp, S. Specific CLK inhibitors from a novel chemotype for regulation of alternative splicing. *Chem. Biol.* **2011**, *18*, 67–76.
- (40) Schmitt, C.; Kail, D.; Mariano, M.; Empting, M.; Weber, N.; Paul, T.; Hartmann, R. W.; Engel, M. Design and synthesis of a library of lead-like 2,4-bisheterocyclic substituted thiophenes as selective Dyrk/Clk inhibitors. *PLoS One* **2014**, *9*, e87851.
- (41) Schmitt, C.; Miralini, P.; Mariano, M.; Hartmann, R. W.; Engel, M. Hydroxybenzothiophene ketones are efficient pre-mRNA splicing modulators due to dual inhibition of Dyrk1A and Clk1/4. *ACS Med. Chem. Lett.* **2014**, *5*, 963–967.
- (42) Becker, A.; Kohfeld, S.; Lader, A.; Preu, L.; Pies, T.; Wieking, K.; Ferandin, Y.; Knockaert, M.; Meijer, L.; Kunick, C. Development of 5-benzylpaullones and paullone-9-carboxylic acid alkyl esters as selective inhibitors of mitochondrial malate dehydrogenase (mMDH). *Eur. J. Med. Chem.* **2010**, *45*, 335–342.
- (43) Kunick, C.; Lauenroth, K.; Leost, M.; Meijer, L.; Lemcke, T. 1-Azakenpaullone is a selective inhibitor of glycogen synthase kinase-3. *Bioorg. Med. Chem. Lett.* **2004**, *14*, 413–416.
- (44) Kunick, C.; Lauenroth, K.; Wieking, K.; Xie, X.; Schultz, C.; Gussio, R.; Zaharevitz, D.; Leost, M.; Meijer, L.; Weber, A.; Jorgensen, F. S.; Lemcke, T. Evaluation and comparison of 3D-QSAR CoMSIA models for CDK1, CDK5, and GSK-3 inhibition by paullones. *J. Med. Chem.* **2004**, *47*, 22–36.
- (45) Kunick, C.; Schultz, C.; Lemcke, T.; Zaharevitz, D. W.; Gussio, R.; Jalluri, R. K.; Sausville, E. A.; Leost, M.; Meijer, L. 2-Substituted paullones: CDK1/cyclin B-inhibiting property and in vitro antiproliferative activity. *Bioorg. Med. Chem. Lett.* **2000**, *10*, 567–569.
- (46) Kunick, C.; Zeng, Z.; Gussio, R.; Zaharevitz, D.; Leost, M.; Totzke, F.; Schächtele, C.; Kubbutat, M. H. G.; Meijer, L.; Lemcke, T. Structure-aided optimization of kinase inhibitors derived from alsterpaullone. *ChemBioChem* **2005**, *6*, 541–549.
- (47) Lahusen, T.; De Siervi, A.; Kunick, C.; Senderowicz, A. M. Alsterpaullone, a novel cyclin-dependent kinase inhibitor, induces apoptosis by activation of caspase 9 due to perturbation in mitochondrial membrane potential. *Mol. Carcinog.* **2003**, *36*, 183–194.
- (48) Leost, M.; Schultz, C.; Link, A.; Wu, Y.-Z.; Biernat, J.; Mandelkow, E.-M.; Bibb, J. A.; Snyder, G. L.; Greengard, P.; Zaharevitz, D. W.; Gussio, R.; Senderowicz, A. M.; Sausville, E. A.; Kunick, C.; Meijer, L. Paullones are potent inhibitors of glycogen synthase kinase-3 β and cyclin-dependent kinase 5/p25. *Eur. J. Biochem.* **2000**, *267*, S983–S994.
- (49) Pies, T.; Schaper, K.-J.; Leost, M.; Zaharevitz, D. W.; Gussio, R.; Meijer, L.; Kunick, C. CDK1-inhibitory activity of paullones depends on electronic properties of 9-substituents. *Arch. Pharm. (Weinheim, Ger.)* **2004**, *337*, 486–492.
- (50) Schultz, C.; Link, A.; Leost, M.; Zaharevitz, D. W.; Gussio, R.; Sausville, E. A.; Meijer, L.; Kunick, C. Paullones, a series of cyclin-dependent kinase inhibitors: synthesis, evaluation of CDK1/ cyclin B inhibition, and in vitro antitumor activity. *J. Med. Chem.* **1999**, *42*, 2909–2919.
- (51) Tolle, N.; Kunick, C. Paullones as inhibitors of protein kinases. *Curr. Top. Med. Chem.* **2011**, *11*, 1320–1332.
- (52) Wieking, K.; Knockaert, M.; Leost, M.; Zaharevitz, D. W.; Meijer, L.; Kunick, C. Synthesis of paullones with aminoalkyl side chains. *Arch. Pharm. (Weinheim, Ger.)* **2002**, *335*, 311–317.
- (53) Zaharevitz, D. W.; Gussio, R.; Leost, M.; Senderowicz, A.; Lahusen, T.; Kunick, C.; Meijer, L.; Sausville, E. A. Discovery and initial characterization of the paullones, a novel class of small-molecule inhibitors of cyclin-dependent kinases. *Cancer Res.* **1999**, *59*, 2566–2569.
- (54) Becker, A.; Kohfeld, S.; Pies, T.; Wieking, K.; Preu, L.; Kunick, C. Synthesis of 11*H*-indolo[3,2-*c*]quinoline-6-carboxylic acids by cascade autoxidation-ring contractions. *Synthesis* **2009**, 1185–1189.
- (55) Ryczak, J.; Papini, M.; Lader, A.; Nasereddin, A.; Kopelyanskiy, D.; Preu, L.; Jaffe, C. L.; Kunick, C. 2-Arylpauullones are selective antitrypanosomal agents. *Eur. J. Med. Chem.* **2013**, *64*, 396–400.
- (56) Maiwald, F.; Benítez, D.; Charquero, D.; Dar, M. A.; Erdmann, H.; Preu, L.; Koch, O.; Hölscher, C.; Loaëc, N.; Meijer, L.; Comini, M. A.; Kunick, C. 9- and 11-substituted 4-azapaullones are potent and selective inhibitors of African trypanosoma. *Eur. J. Med. Chem.* **2014**, *83*, 274–283.
- (57) de Graaf, K.; Czajkowska, H.; Rottmann, S.; Packman, L. C.; Lilischkis, R.; Luscher, B.; Becker, W. The protein kinase DYRK1A phosphorylates the splicing factor SF3b1/SAP155 at Thr434, a novel in vivo phosphorylation site. *BMC Biochem.* **2006**, *7*, 7.
- (58) Göckler, N.; Jofre, G.; Papadopoulos, C.; Soppa, U.; Tejedor, F. J.; Becker, W. Harmine specifically inhibits protein kinase DYRK1A and interferes with neurite formation. *FEBS J.* **2009**, *276*, 6324–6337.
- (59) Mariano, M.; Schmitt, C.; Miralini, P.; Catto, M.; Hartmann, R. W.; Carotti, A.; Engel, M. First selective dual inhibitors of tau phosphorylation and beta-amyloid aggregation, two major pathogenic

mechanisms in Alzheimer's disease. *ACS Chem. Neurosci.* **2014**, *5*, 1198–1202.

(60) Soundararajan, M.; Roos, A. K.; Savitsky, P.; Filippakopoulos, P.; Kettenbach, A. N.; Olsen, J. V.; Gerber, S. A.; Eswaran, J.; Knapp, S.; Elkins, J. M. Structures of Down syndrome kinases, DYRKs, reveal mechanisms of kinase activation and substrate recognition. *Structure* **2013**, *21*, 986–996.

(61) Wilcken, R.; Zimmermann, M. O.; Lange, A.; Joerger, A. C.; Boeckler, F. M. Principles and applications of halogen bonding in medicinal chemistry and chemical biology. *J. Med. Chem.* **2013**, *56*, 1363–1388.

(62) Voth, A. R.; Ho, P. S. The role of halogen bonding in inhibitor recognition and binding by protein kinases. *Curr. Top. Med. Chem.* **2007**, *7*, 1336–1348.

(63) Huber, K.; Brault, L.; Fedorov, O.; Gasser, C.; Filippakopoulos, P.; Bullock, A. N.; Fabbro, D.; Trappe, J.; Schwaller, J.; Knapp, S.; Bracher, F. 7,8-Dichloro-1-oxo- β -carboline as a versatile scaffold for the development of potent and selective kinase inhibitors with unusual binding modes. *J. Med. Chem.* **2012**, *55*, 403–413.

(64) Poznański, J.; Shugar, D. Halogen bonding at the ATP binding site of protein kinases: preferred geometry and topology of ligand binding. *Biochim. Biophys. Acta* **2013**, *1834*, 1381–1386.

(65) Armarego, W. L. F.; Chai, C. L. L. *Purification of Laboratory Chemicals*; MPG Books: Bodmin, Cornwall, U.K., 2003.

(66) Kunick, C. Synthese [b]-kondensierter azepindione durch dealkoxycarbonylierung. *Arch. Pharm. (Weinheim, Ger.)* **1991**, *324*, 579–581.

(67) Egert-Schmidt, A.-M.; Dreher, J.; Dunkel, U.; Kohfeld, S.; Preu, L.; Weber, H.; Ehlert, J. E.; Mutschler, B.; Totzke, F.; Schächtele, C.; Kubbutat, M. H. G.; Baumann, K.; Kunick, C. Identification of 2-anilino-9-methoxy-5,7-dihydro-6H-pyrimido[5,4-d][1]benzazepin-6-ones as dual PLK1/VEGF-R2 kinase inhibitor chemotypes by structure-based lead generation. *J. Med. Chem.* **2010**, *53*, 2433–2442.

(68) Leclerc, S.; Garnier, M.; Hoessel, R.; Marko, D.; Bibb, J. A.; Snyder, G. L.; Greengard, P.; Biernat, J.; Wu, Y.-Z.; Mandelkow, E.-M.; Eisenbrand, G.; Meijer, L. Indirubins inhibit glycogen kinase-3 β and CDK5/p25, two protein kinases involved in abnormal tau phosphorylation in Alzheimer's disease—a property common to most CDK inhibitors? *J. Biol. Chem.* **2001**, *276*, 251–260.

(69) Primot, A.; Baratte, B.; Gompel, M.; Borgne, A.; Liabeuf, S.; Romette, J. L.; Costantini, F.; Meijer, L. Purification of GSK-3 by affinity chromatography on immobilised axin. *Protein Expression Purif.* **2000**, *20*, 394–404.

(70) Reinhardt, J.; Ferandin, Y.; Meijer, L. Purification of CK1 by affinity chromatography on immobilised axin. *Protein Expression Purif.* **2007**, *54*, 101–109.

(71) Kabsch, W. XDS. *Acta Crystallogr., Sect. D: Biol. Crystallogr.* **2010**, *66*, 125–132.

(72) Batty, T. G.; Kontogiannis, L.; Johnson, O.; Powell, H. R.; Leslie, A. G. iMOSFLM: a new graphical interface for diffraction-image processing with MOSFLM. *Acta Crystallogr., Sect. D: Biol. Crystallogr.* **2011**, *67*, 271–281.

(73) Collaborative Computational Project, Number 4. The CCP4 suite: programs for protein crystallography. *Acta Crystallogr., Sect. D: Biol. Crystallogr.* **1994**, *50*, 760–763.

(74) McCoy, A. J.; Grosse-Kunstleve, R. W.; Adams, P. D.; Winn, M. D.; Storoni, L. C.; Read, R. J. Phaser crystallographic software. *J. Appl. Crystallogr.* **2007**, *40*, 658–674.

(75) Emsley, P.; Lohkamp, B.; Scott, W. G.; Cowtan, K. Features and development of Coot. *Acta Crystallogr., Sect. D: Biol. Crystallogr.* **2010**, *66*, 486–501.

(76) Murshudov, G. N.; Vagin, A. A.; Dodson, E. J. Refinement of macromolecular structures by the maximum-likelihood method. *Acta Crystallogr., Sect. D: Biol. Crystallogr.* **1997**, *53*, 240–255.

(77) Painter, J.; Merritt, E. A. Optimal description of a protein structure in terms of multiple groups undergoing TLS motion. *Acta Crystallogr., Sect. D: Biol. Crystallogr.* **2006**, *62*, 439–450.

(78) Davis, I. W.; Leaver-Fay, A.; Chen, V. B.; Block, J. N.; Kapral, G. J.; Wang, X.; Murray, L. W.; Arendall, W. B., 3rd; Snoeyink, J.;

Richardson, J. S.; Richardson, D. C. MolProbity: all-atom contacts and structure validation for proteins and nucleic acids. *Nucleic Acids Res.* **2007**, *35*, W375–W383.

(79) Jones, G.; Willett, P.; Glen, R. C.; Leach, A. R.; Taylor, R. Development and validation of a genetic algorithm for flexible docking. *J. Mol. Biol.* **1997**, *267*, 727–748.

(80) *Molecular Operating Environment (MOE)*; Chemical Computing Group Inc. (1010 Sherbrooke St. W, Suite 910, Montreal, Quebec, Canada, H3A 2R7), 2014.